Article

Acoustic lattice resonances and generalised Rayleigh–Bloch waves

Check for updates

G. J. Chaplain [1] ✉, S. C. Hawkins [2], M. A. Peter [3,4], L. G. Bennetts [5] & T. A. Starkey [1]

The intrigue of waves on periodic lattices and gratings has resonated with physicists and mathematicians alike for decades. In-depth analysis has been devoted to the seemingly simplest array system: a one-dimensionally periodic lattice of two-dimensional scatterers embedded in a dispersionless medium governed by the Helmholtz equation. We investigate such a system and experimentally confirm the existence of a new class of generalised Rayleigh–Bloch waves that have been recently theorised to exist in classical wave regimes, without the need for resonant scatterers. Airborne acoustics serves as such a regime and we experimentally observe the first generalised Rayleigh–Bloch waves above the first cut-off, i.e., in the radiative regime. We consider radiative acoustic lattice resonances along a diffraction grating and connect them to generalised Rayleigh–Bloch waves by considering both short and long arrays of non-resonant 2D cylindrical Neumann scatterers embedded in air. On short arrays, we observe finite lattice resonances under continuous wave excitation, and on long arrays, we observe propagating Rayleigh–Bloch waves under pulsed excitation. We interpret their existence by considering multiple wave scattering theory and, in doing so, unify differing nomenclatures used to describe waves on infinite periodic and finite arrays and the interpretation of their dispersive properties.

One-dimensionally periodic lattices (with appropriate boundary conditions on the scatterers[1]) support surface waves that propagate along and exponentially decay away from the lattice. These exist under many guises for both scalar and vector wave regimes from acoustics and electromagnetism, to linear water waves and elasticity[2–5]. Distinct from naturally occurring interfacial surface waves (e.g., Rayleigh, Stonely, and Scholte waves, or surface plasmon polaritons), the waves we allude to owe their existence to the underlying embedded periodic lattice and are thus commonly termed Rayleigh–Bloch (RB) waves; they exist on infinite lattices, with the criterion for their existence having been analysed in the context of functional analysis for some time[2,6,7]. In particular, they differ from pure Bloch waves that exist in cells which are bounded (e.g., an infinite 2D phononic crystal), as RB waves exist in 1D lattices with an unbounded unit cell, resembling a strip or ribbon[8].

The finite width of the periodic cells (or strips) tiling physical space gives rise to multiple 'cut-offs': wavevectors in reciprocal space at the Brillouin Zone boundaries (BZBs)[9], with associated frequencies determined by the dispersion relation of the array. The wavelengths of the associated Bloch solutions become integer half-multiples of the cell width and standing wave solutions are formed (the Bragg condition). For a 1D periodic lattice embedded in a dispersionless medium, RB waves within the first BZ (below the first cut-off) are constrained to lie below the sound-line (in acoustics), the gradient of which gives the velocity of free-space acoustic waves. As they lie below the sound-line, RB waves cannot be excited by plane waves on an infinite grating, but they can on semi-infinite and finite gratings[3,10,11]. For symmetric scatterers, RB waves in the standing-wave limit are equivalent to so-called Neumann modes[2]. In a finite array, they are closely related to localised lattice resonances, which have the form of near-standing-wave solutions just below the Neumann-mode frequency created by constructive interference between RB waves after end reflections[11]; the frequency at which they exist is often predicted by analysis of the infinite periodic picture.

Notably, there has been more recent mathematical consideration of RB waves that exist above the first cut-off[12]. They exist in the radiative (leaky) regime, i.e., above the sound line, and can therefore couple to plane waves. In particular, a second kind of RB mode exists above the first cut-off in which their wavenumbers become complex-valued. They exist *both* above the cut-off and on finite arrays. The connection between these "generalised" RB waves and finite lattice resonances has been explored[13]. At their discovery,

[1]Centre for Metamaterial Research and Innovation, Department of Physics and Astronomy, University of Exeter, Exeter, UK. [2]School of Mathematical and Physical Sciences, Macquarie University, Sydney, NSW, Australia. [3]Institute of Mathematics, University of Augsburg, Augsburg, Germany. [4]Centre for Advanced Analytics and Predictive Sciences (CAAPS), University of Augsburg, Augsburg, Germany. [5]School of Computer and Mathematical Sciences, University of Adelaide, Adelaide, Australia. ✉e-mail: g.j.chaplain@exeter.ac.uk

they were termed extended RB waves[13] due to where they exist in terms of the position of the cut-off. Here we denote them generalised RB waves so to avoid confusion with their extent in decay away from the array. They exist over a range of parameter intervals that we explore here for the first time experimentally, viz. in audible acoustics. The modes of open systems are commonly termed quasi-normal modes (QNMs) characterised by complex eigenfrequencies[14], that naturally occur above the first cut-off. These have received much attention in resonant systems, particularly in the field of plasmonics; QNMs form a complete basis and are thus used to represent waves spectrally in resonant systems[15]. Their mathematical intricacies are still of interest[16,17], and are commonly utilised in open electromagnetic systems, including periodic gratings[18–20] (and recently in platonics[21]). Above the cut-off, however, not all modes are QNMs; special cases being the higher-order Neumann and Dirichlet modes (see below) with purely real point eigenvalues that exist for very particular parameter combinations, embedded in the continuous spectrum[12]. As such, they are often termed bound states in the continuum (BIC)[22]. The generalised RB waves we consider here are not BICs, but very close to (sometimes referred to as quasi-BICs or leaky resonances[23,24]).

In this article, we seek to investigate the behaviour of lattices for acoustic waves in the regime above the first cut-off for short arrays with a few tens of scatterers (under continuous wave excitation) and long arrays with several tens of scatterers (under pulsed excitation), making the connection to generalised RB waves. We demonstrate that their existence depends on the aspect ratio between scatterer radius and cell width, as predicted in ref. 13, and justify this with multiple wave scattering (MWS) theory.

In Fig. 1, we provide motivation for this study by showing experimental observations of acoustic lattice resonances above the first cut-off as predicted in ref. 13, for a finite array of 11 scatterers. The frequencies of the resonances are close to the BZBs (marked by dashed vertical lines).

Figure 1a, c compare finite element(FE) models to the theoretical predictions of ref. 13, and FE models to experiment respectively (methods detailed below) for the case of radius to separation $r/a = 0.15$. In Fig. 1b, d, we show analogous results, up to the first cut-off, but for the case where $r/a = 0.35$. By considering the connection to generalised RB waves, and intuition gained from MWS theory, we shall show that the first resonance above the cut-off in this configuration does not exist, as predicted[13]; in general, higher-order resonances may cut back on and this requires tracking the complex eigenvalues[25]. The FE simulations in Fig. 1c, d include a small amount of disorder in the centre position of the cylinders to reflect the experimental limitations (see below), which is known not to localise the RB wave[26] i.e., the resonances observed are not spatially localised to the vicinity of the source (Anderson localisation[27]), or dissipation (the FE solutions contain no loss) and instead originate as predicted in ref. 13.

In Fig. 1e, f, we show (lossless) FE frequency domain simulations of the normalised acoustic pressure, showing the lattice resonances, for the cases of $r/a = 0.15$ and $r/a = 0.35$, respectively. A point source excitation is to the left of the array, at the corresponding frequencies marked by the circles in (a,b). In these examples, the radius is fixed and the spacing is altered, as in the experiment. In Fig. 1g, h, we show multiple wave scattering simulations for the same configurations, but this time with the spacing remaining fixed and the radius changing. Coupling to radiation of the resonance above the first cut off is evident in (e,g).

Lattice resonances above the cut-off have been investigated for systems of *resonant* scatterers for many years, particularly in the active field of plasmonics[28–32] with leaky antennas serving as an attractive application[33,34]. However, the collective electromagnetic oscillations in plasmonics differ fundamentally from the acoustic lattice oscillations we observe here; in plasmonics the scatterers have their own individual resonant profiles described by well-defined dielectric functions, given by for example the
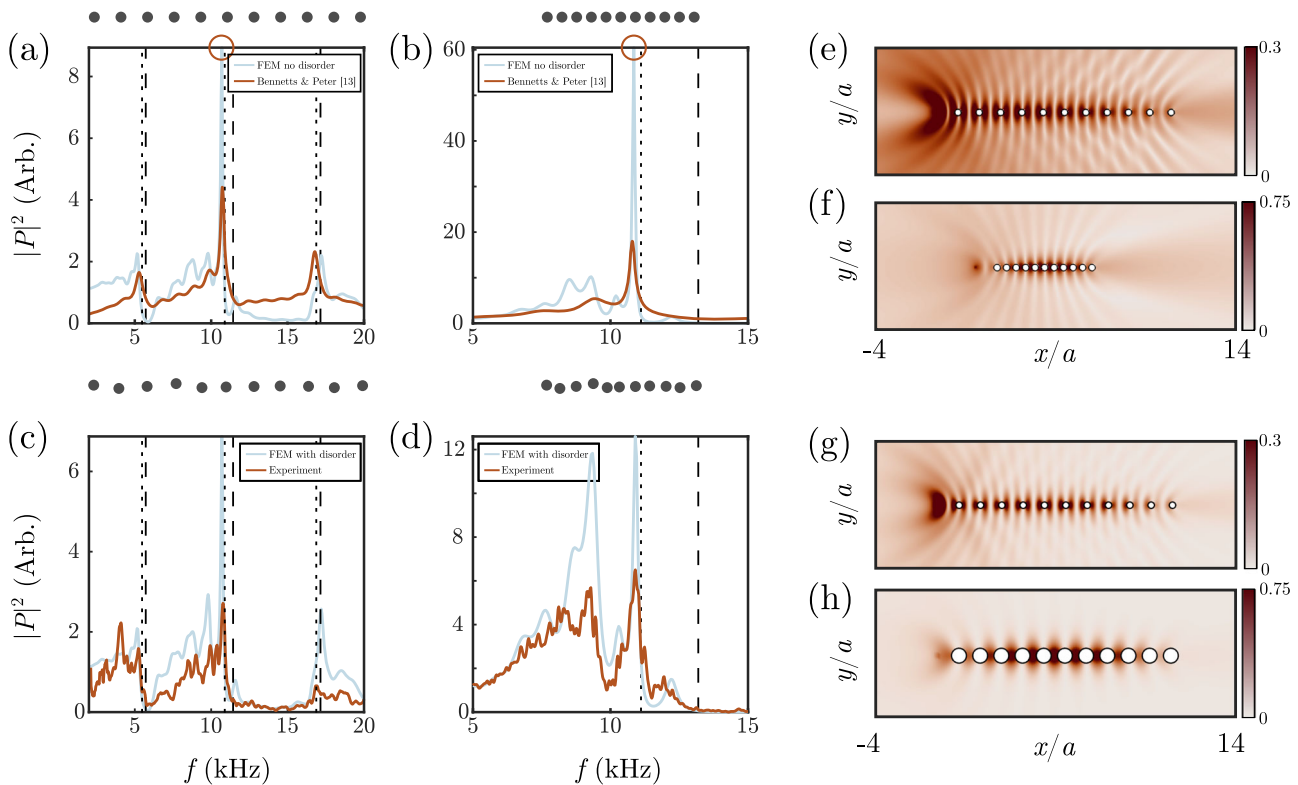

Fig. 1 | Acoustic Lattice Resonances. a, b Normalised load on central cylinder from the finite element method (FEM) (blue—with point source) and method in ref. 13 (orange—with plane wave source), for an 11 scatterer array with $r/a = 0.15$, 0.35. **c, d** Analogous finite element (FE) curves (blue) on disordered array and experimental results (orange). The band edges and standing-wave frequencies from the infinitely periodic analogue are shown in dashed and dotted lines, respectively. Array schematics shown above panels. **e, f** Normalised absolute acoustic pressure field (colorscale) from FE method at frequencies marked with circle in (**a, b**) respectively. **g, h** Analogous multiple wave scattering simulations but with radii scaled rather than separation. Point source excitation is to the left of each array.

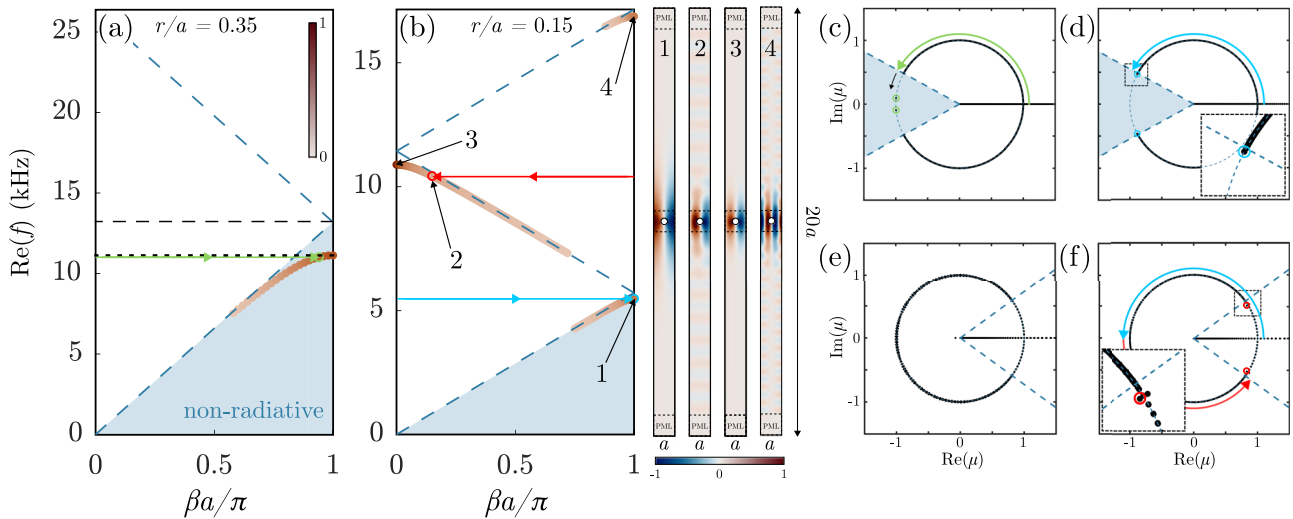**Fig. 2 | Dispersion curves and Rayleigh–Bloch (RB) modes. a, b** Finite element (FE) dispersion curves for differing aspect ratio (radius to unit cell width) $r/a = 0.35$, 0.15, respectively. The sound line is shown in dashed blue with non-radiative regime highlighted; dotted and dashed black lines correspond to standing-wave and band-edge frequencies, respectively, in Fig. 1b, d. Colourscale indicates localisation to the array (Finite Element Methods section). Mode-shapes show RB and generalised RB modes numbered in (**b**). Neumann and Dirichlet trapped modes (purely real eigenfrequencies) are labelled 1 & 3, respectively. **c–f** Representations of dispersion spectra as complex eigensolutions μ (black points) for $r/a = 0.35$ (**c, e**) and 0.15 (**d, f**). Coloured arrows show direction around the continuous spectra along the unit circle, corresponding to a fixed frequency and altering RB wavenumber β in (**a, b**)—the real parts of the eigensolutions are highlighted with corresponding colours in (**a, b**). Below the cut-off, the eigensolutions lead the unit circle (black arrow), as in (**c, d**). The first generalised RB mode above the cut-off appears as complex solutions off the unit circle for large aspect ratio (**f**) that are not present in (**e**). Dashed boxes in (**d, f**) show a zoom near the cut-offs.

Drude model[35]. We consider classical, linear acoustic pressure waves on a 1D periodic lattice of Neumann (impenetrable, sound-hard) cylinders at audible frequencies in air. We experimentally observe collective acoustic lattice resonances above the (first) cut-off that arise due to radiative coupling of scattered waves by the grating. This is also viewed numerically with both the finite element method and semi-analytical multiple wave scattering theory, leading to a unification of nomenclature between the methods of analysis. Finally, we elucidate the physical mechanism driving these resonances, and how this manifests itself in their experimental detection by considering scatterer polarisability.

Results

Acoustic Rayleigh–Bloch waves

To find acoustic RB waves, we seek solutions, ϕ, of the 2D Helmholtz equation

$$(\Delta + k^2)\phi = 0, \qquad (1)$$

in the xy-plane with sound-hard (Neumann) boundary conditions applied on periodically spaced cylindrical scatterers with boundary Γ, separation a and radius r, that satisfy both radiation and Bloch conditions, i.e.,

$$\begin{cases} \frac{\partial \phi}{\partial \boldsymbol{n}} = 0 & \text{on } \Gamma, \\ \phi \to 0 & \text{as } |y| \to \infty, \\ \phi_R = \exp(iR\beta)\phi_0, \\ \partial_x \phi_R = \exp(iR\beta)\partial_x\phi_0, \end{cases} \qquad (2)$$

where $\boldsymbol{n}$ is the outward surface normal, ϕ_0 is the solution in the fundamental cell and ϕ_R is the solution in the Rth cell at a distance $R = na$ for $n \in \mathbb{Z}$. Solutions to this problem are known as pure Rayleigh–Bloch surface waves[7] with the prescribed values of k^2 at which they occur being eigenvalues of the operator $-\Delta$ subject to (2). As is often the case, a non-dimensional form is adopted and, as such, k is a wavenumber that acts as a proxy for a prescribed angular frequency. With this, β represents the RB wavenumber, i.e., the component of the wavevector parallel to the array. Given the translational invariance of the unit strip, we are free to fix either real k or β and solve for the other. This distinction is not clear-cut in non-Hermitian systems and, according to generalised Brillouin Zone theory, both k and β should be treated as complex and solved for simultaneously[36,37], which has implications in acoustics[38,39]. Here however, in an analogy to optical modes[20], we may define β and compute the complex values as a function of real frequency k; for guided modes (i.e., RB modes below the cut-off), β is real and only becomes complex due to absorption and/or leakage[20]. Alternatively, one may fix real β and solve for complex k (the QNMs) that exist with or without invariance; in some cases, it is advantageous to solve instead for complex material parameters, e.g., permittivity[40,41]. A useful distinction between guided modes and QNMs is present in ref. 19 in the context of surface plasmons (although, in acoustics, there only exists analogues to their spoof counterparts). The differences in this convention typically arise between mathematicians and physicists, e.g., the methods in ref. 13 and ref. 42 respectively, and can be influenced by physical experiments, e.g., driving with real frequency or spatially separated sources (fixing real β). Throughout, we shall use a mixture of both and highlight the advantages in finding and interpreting generalised RB waves.

We are careful to note here that the final two boundary conditions in (2) represent the Floquet–Bloch conditions across the unit cell, satisfied only in the infinite problem. Near the cut-off frequencies the periodic boundary conditions are often referred to as the Neumann and Dirichlet conditions *across* the cell. The corresponding solutions being Neumann and Dirichlet modes, respectively (labelled '1' and '3' respectively in Fig. 2). This nomenclature originates from trapped waves in a channel with such boundaries on the sidewalls[13,43–45] and are also sometimes referred to as the periodic and anti-periodic conditions across the cell[46]; these modes have uses in inferring bandgap frequencies akin to ref. 47. We make this point to avoid confusion; when Neumann (sound-hard) boundary conditions are referred to, it is on the boundary of the scatterers Γ and not across the unit cell. Indeed, an infinite array of Dirichlet scatterers does not support RB waves[1].

In Fig. 2, we show two common interpretations of the dispersion relations for infinite arrays. The parallel component of the wavevector along the axis (the RB wavenumber β) is related to the free-space wavevector of magnitude $k_0 = \omega/c$, with c the speed of sound through $\beta = k_0 \sin\theta$, where θ prescribes the angle relative to the normal to the array axis. In Fig. 2a, b, the
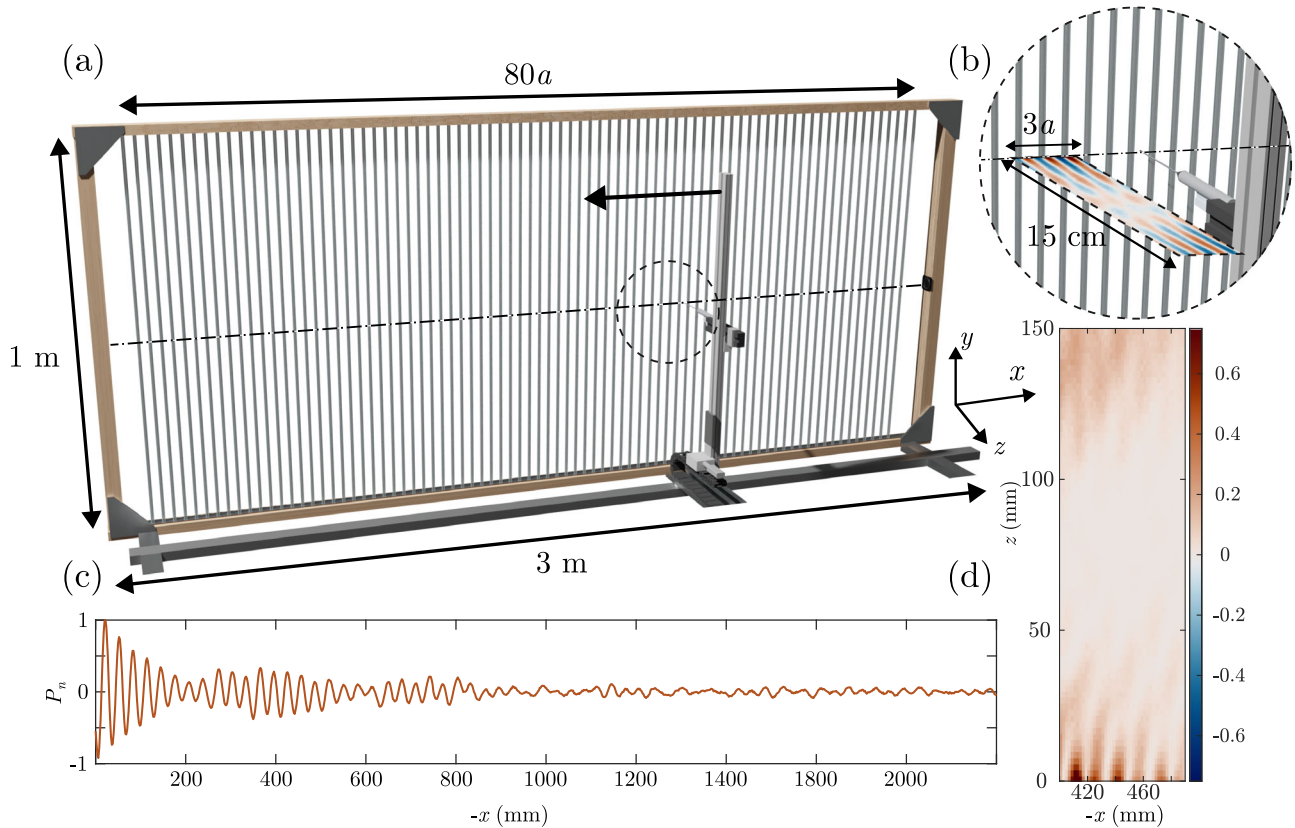
Fig. 3 | Experimental setup and example scans. a Scanning xyz-stage and long array of 80 cylindrical acrylic rods in laser-cut stencils that set aspect ratio r/a. Dash-dotted line shows scan path and arrow shows direction in $-x$. **b** Zoom of area scan and example spatial distribution showing normalised real pressure amplitude at a frequency of 10.9 kHz, for $r/a = 0.15$. **c** Normalised real pressure Fourier amplitude at 10.9 kHz evaluated along scan line. **d** Corresponding time-averaged absolute pressure field area scan, highlighting localisation to the array; the decay due to radiative loss evident in (**c**, **d**) with beating in amplitude occurring due to interference with source (that decays with distance as expected).

dispersion curves for RB waves below and above the cut-off are evaluated with finite elements. Here, the RB waves below the first cut-off are highlighted in the non-radiative regime $\beta > k_0$ (shown in blue). They exist, with varying degrees of dispersion, for any aspect ratio r/a. Modes beyond the non-radiative regime, i.e., above the first cut-off, are shown to exist below $r/a < 0.33$ as predicted by ref. 13 and are introduced by the perfectly matched layers (PMLs)[18]. Mode shapes are shown in the unit-strip at four frequencies, labelled in Fig. 2b. Modes 1&3 are the Neumann and Dirichlet trapped modes respectively, with purely real eigenfrequencies. Modes 2&4 represent generalised RB waves that have complex eigenfrequencies, evidenced by the coupling to the far-field.

In Fig. 2c–f, we adopt the representation from[13], and show the RB waves through the introduction of the parameter μ: the eigenvalues of the transfer operator that describes propagation along the array (method outlined in ref. 26). For RB waves, the eigenspectra take the form $\mu = \exp(\pm iR\beta)$ and RB modes below the cut-off arise as eigenvalues that lead the unit circle in the complex plane in the non-radiative regime (green points in Fig. 2c). Those that lie on the unit circle are solutions for propagating background waves forming the continuous spectra. This corresponds to following β at a fixed frequency, highlighted by the green arrow in Fig. 2a, reaching the highlighted eigenvalue in green. At the first cut-off, the unit circle closes at $\mu = -1$ ($\beta R = \pi$). Above the first cut-off $\beta > \pi/a$ (now in a higher BZ we see as band folded in Fig. 2b), the continuous spectrum overlaps itself and generalised RB waves with complex wavenumber appear as pairs of eigenvalues off the unit circle, shown in Fig. 2f. When the aspect ratio becomes large, i.e., the cylinder occupies a larger fraction of the unit strip, these modes above the cut-off cease to exist[25]; they are not present in (e) for the case of $r/a = 0.35$. In the following sections, we detail this observation experimentally and explain this phenomenon in terms of multiple wave

scattering theory and the polarisability of the scatterers, in particular, matching the scattering amplitudes of the radiative wave functions with the symmetries of the eigenmodes supported by the array. We elucidate this for the first generalised RB mode above the cut-off that approaches the Dirichlet trapped mode[12].

Experimental Results

To observe the generalised RB waves above the cut-off experimentally, we consider two arrays with aspect ratios $r/a = 0.15$ and 0.35, fabricated by fixing acrylic rods ($r = 4.5$ mm) in slotted laser-cut templates mounted within a timber frame. We design two array lengths: a set of 11 rods, and a much larger array of 80 rods to approximate the infinite regime and to achieve the required resolution in reciprocal space. The rods are 1 m in height and a loudspeaker was mounted within the frame, at the rod midheight. Measurements are extracted from the mid-plane to approximate an open 2D array. A schematic of the array and scanning equipment is shown in Fig. 3a and detailed experimental procedures are outlined in the Methods section.

In Fig. 1, we show the results for the case of 11 cylinders under continuous wave excitation. Figure 1a, b shows the normalised load on the central cylinder, evaluated through frequency domain FE simulations, and the method outlined in ref. 13. Clear peaks can be seen that correspond to collective lattice resonances with frequencies close to the cut-offs (i.e., the band edges of the infinitely periodic case, shown by the dashed vertical lines). Also shown are the predicted standing-wave solutions from the corresponding infinite array (e.g., the frequency of modes 1, 3 etc., extracted from the dispersion curves in Fig. 2b) as dotted vertical lines.

In practice, the rods are nonuniformly bowed in the manufacturing procedure. To explore the impact of this, in Fig. 1c, d, we show a similar
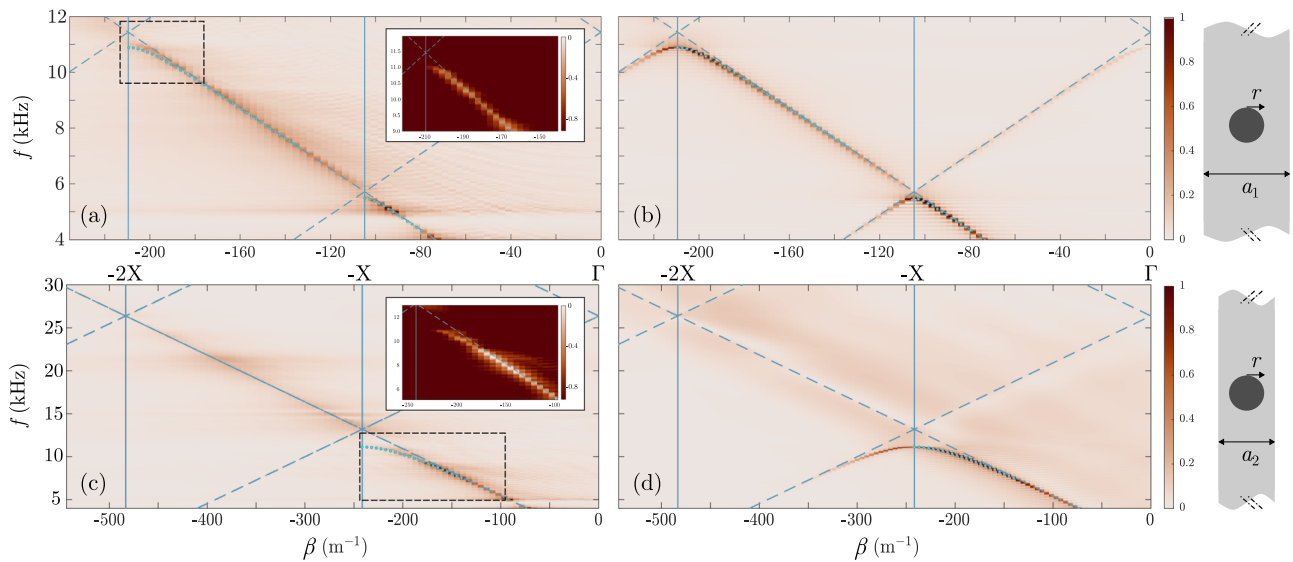
Fig. 4 | Experimental and numerical observation. a, b Normalised experimental and numerical Fourier spectra respectively from line scans for the configuration of 80 rods with $r/a_1 = 0.15$. The mode above the cut-off is predominant, as predicted in Figs. 1c and 2b. **c, d** Show similar spectra but for the ratio $r/a_2 = 0.35$—no mode above the cut-off is supported. Insets show logarithm of the Fourier spectra in the regions highlighted by the dashed rectangles, where the peeling of the mode off the sound-line is more visible. Overlaid points are from the eigenfrequency study (Fig. 2). Schematics show the unit strips.

comparison, but this time between FE and experiments, and in the FE case disorder has been added to the scatterer positions (in the form of normally distributed random noise). As expected, RB waves still exist in the case of disorder[26]. The pressure amplitude is extracted at positions near the central rod with and without the array, averaged and normalised. There is good agreement between the predicted positions of the frequencies of the resonances, and their oscillatory behaviour before the cut-off[18]. They closely align to the eigensolutions for the standing waves in the infinitely periodic case, indicating the nature of their existence through reflections of generalised RB waves.

The RB waves are clearly observed in the longer array. We perform pulsed measurements along an array with 80 rods to approximate an infinite array when excited with an acoustic pulse. To obtain the dispersion spectra, the microphone is scanned along the full sample length in the propagation direction. To visualise the wave-field, small area pressure fields maps are shown on a plane normal to the rods in the propagation direction (150 mm × 3 unit cells) in Fig. 3b. A zoom of the absolute time-averaged pressure field highlights localisation to the array. In Fig. 3c, we show the normalised real pressure frequency response near the second cut-off, at 10.9 kHz, showing propagation of a decaying generalised RB wave. Due to the intrinsic losses of the fluid and the leaky coupling to radiation, the amplitude decays along the array and as such reflections from the end are minimal; the resonances observed in Fig. 1 are not observed due to the pulsed excitation as steady state is not reached.

In Fig. 4, we show the frequency spectra obtained by Fourier analysis (see Methods). Dispersion spectra are normalised by the maximum value at each frequency for each aspect ratio. Figure 4a, c and insets show the logarithmic spectra to aid visualisation of the dispersion. In the case of high aspect ratio, as predicted, generalised RB waves do not exist and are only detected when the spacing between the cylinders is sufficiently large. In Fig. 4b, d we show the numerical counterpart to the experiment, the results of similar Fourier analysis of a 2D frequency domain simulation using FE. The array is excited by a point source at the same distance away from the array to the loudspeaker. In this case, the zero group velocity mode at the band edge is detected as viscous losses are not included. Overlaid in both cases are the corresponding eigenfrequencies from the infinite dispersion problem (Fig. 2) showing excellent agreement.

Discussion

Here, we outline a physical reasoning for why generalised RB waves do not exist at high aspect ratios. To do so, we turn to language that is commonplace within electromagnetism and plasmonics, and now the metamaterial community in general, and focus on the polarisability of the scatterers.

Electromagnetic polarisability is a measure of how easily the charge distribution of a scatterer, be it a molecule or metallic nano-particle, may be distorted by an external electric field[49] and is thus related to the scattering strength of the material. In acoustics, an analogous notion of polarisability exists that relates the dipole and monopole scattering strengths (moments) to the particle velocity and local pressure[50]. Measuring the tensor that governs these interactions has received attention in acoustics where the scatterers are considered acoustically small (i.e., $ka \ll 1$)[51,52]. This is particularly relevant for sub-wavelength metamaterials but is not the case for the generalised RB waves, where, by definition, they have wavelengths commensurate with (and smaller than) the unit strip width. As such, we turn to multiple wave scattering (MWS) theory to elucidate the scattering profile of a single scatterer, then a pair of scatterers, and thereby inductively inferring the behaviour of the grating composed of many scatterers; this is commonplace in plasmonics, where the polarisabilty of a single metallic particle is used to obtain the scattering cross-section of an array[53,54]. We do so using the T-matrix method[55], which has had recent attention in metamaterial applications[56], to evaluate the radiating wavefunction expansion coefficients of the scattered field.

Recall (1), the Helmholtz equation for a scalar monochromatic field (assuming $\exp(-i\omega t)$ time dependence). In MWS theory, the field ϕ is split into an incident field ϕ^{inc} that interacts with scatterers Γ, to induce a scattered field ϕ^{scat}, both satisfying (1) such that $\phi = \phi^{\text{inc}} + \phi^{\text{scat}}$. The scattered field must also satisfy, for an unbounded domain as we assume here, the Sommerfeld radiation condition[57]

$$\lim_{\rho \to \infty} \sqrt{\rho}\left(\frac{\partial \phi^{\text{scat}}}{\partial \rho} - ik\phi^{\text{scat}}\right) = 0, \qquad (3)$$

which, in 2D, has the far field

$$\phi^{\infty}(\theta) = \lim_{\rho \to \infty} \sqrt{\rho}\, e^{-ik\rho}\phi^{\text{scat}}(\boldsymbol{r}, \theta), \qquad (4)$$
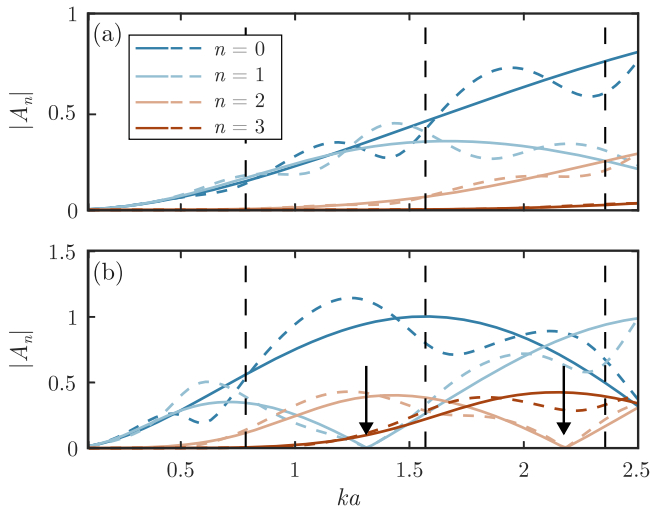
Fig. 5 | Radiating wavefunction expansion coefficients. a Coefficients of a single scatterer (solid lines) and for the first of a pair of scatterers (dashed) for fixed $r/a = 0.15$. **b** Corresponding curves for $r/a = 0.35$. Cut-offs marked by vertical dashed lines (increasing n left to right).

where $\rho = |\mathbf{r}|$. Solving for the field ϕ^{scat} then requires suitable boundary conditions to be imposed on Γ. We turn to expansions in regular and radiating wavefunctions[55]

$$\hat{\phi}_n(\mathbf{r}, \theta) = J_{|n|}(k\rho)e^{in\theta},$$
$$\phi_n(\mathbf{r}, \theta) = H_{|n|}^{(1)}(k\rho)e^{in\theta},$$

$$(5)$$

with $n \in \mathbb{N}$. J_n and $H_n^{(1)}$ are the first-kind Bessel and Hankel functions of order n respectively, such that

$$\phi^{\text{inc}} = \sum_n f_n \hat{\phi}_n,$$
$$\phi^{\text{scat}} = \sum_n A_n \phi_n,$$

$$(6)$$

where f_n and A_n are expansion coefficients, and f_n are typically known, and are known analytically for common incident waves such as plane waves. Numerically evaluating these requires truncation in the summation; the T-matrix method enables numerically stable computation of these coefficients[58], ultimately providing insight into the coupling strength between scatterers.

In Fig. 5, we plot the radiating wave function expansion coefficients of (i) the scattered field of a single cylindrical scatterer (solid lines) and (ii) the coefficients for the first scatterer in a system of two scatterers separated by a (dashed lines). In Fig. 5a, we show the evolution of the expansion coefficient amplitude as we vary ka for fixed radius, corresponding to $r/a = 0.15$. For both the single and pair of scatterers, the expansion coefficients $|A_n|$ are non-zero near the nth cut-offs of the infinite regime (marked by dashed vertical lines). Considering the first generalised RB wave, the scatterers are sufficiently separated so that the dipole-like field can exist between the scatterers and they hence couple. Near the second cut-off, the amplitude of $|A_1| > |A_0|$ for the pair of scatterers, which agrees with the observations in Figs. 1c, 2b and 4a that show this is the predominant mode. Examining the behaviour of the scattering coefficients, as we increase the number of particles in the array, is analogous to considering the increased scattering cross section of arrays of e.g., resonant particles in plasmonics[54].

Contrasting this to Fig. 5b, where $r/a = 0.35$, we see that near the nth cut-off frequencies the corresponding $|A_n|$ vanishes (marked by black arrows) for the case of a single scatterer *and* in the case of a pair of scatterers. The first scatterer cannot couple to the next with these radiating moments. By extension, considering many scatterers, a generalised RB wave cannot exist;

the overlap integral (inner product) of the scattered field and that of the eigenmodes of the array vanishes and the modes are not supported.

As an example, consider the case of the first generalised RB wave above the cut-off, which approaches the Dirichlet trapped mode ($\beta \equiv 0^{12}$), i.e., mode 3 in Fig. 2. The dominant symmetry requires a dipole-like field between the scatterers; this is not supported when $|A_1| = 0$. At higher frequencies, $|A_1|$ is non-zero once more, but the next generalised RB wave requires matching to the quadrupole moment, but again we see near the cut-off $A_2 = 0$. For this reason, at large aspect ratios (e.g., Figs. 1d and 2a) we do not see generalised RB waves. One could also consider asymptotic analysis of the gap as it becomes narrow for large aspect ratios[59,60].

Conclusion

Analysis of finite gratings is a well-trodden path, and their behaviour is often inferred from the infinitely periodic case, even with a very low number of repeat periods. This is commonplace across many wave regimes and has had success in antenna engineering[61,62], with the validity of the periodic approach still receiving attention in the design of metamaterials[63,64]. Waves on finite and semi-infinite lattices are often labelled as RB waves, as is the case for electromagnetic waves on gratings[65,66], spoof surface plasmons[67,68], water waves with depth dependence[3], loaded thin elastic plates and in-plane elastic voids[5,8,69], or acoustic surface waves[42,70,71].

Here, we have experimentally observed generalised RB waves above the first cut-off that manifest as acoustic lattice resonances confined to a diffraction grating. We considered 2D arrays of cylindrical Neumann scatterers embedded in air, forming both small and large-scale acoustic gratings for airborne sound in the audible frequency range. The first generalised RB mode was shown to exist over a range of frequencies for an example aspect ratio predicted by[13]. Generalised RB modes do not exist when the aspect ratio becomes large and the physical justification of this was presented in the context of multiple wave scattering theory; the scatterers do not support the radiating scattering wavefunctions which couple dipolar (and higher order) interactions. As we operate above the first cut-off, the supported waves couple through radiation and are inherently lossy.

In airborne acoustics, we are afforded the luxury of being able to achieve both continuous wave and pulsed excitations that permit the excitation of collective acoustic lattice resonances on short arrays and propagating generalised RB waves on long arrays respectively. In doing so, we have demonstrated that they are one and the same and that their interpretation is unified through the analogue of polarisability of the scatterers and the gaps between them.

Methods
Finite Element Methods
Dispersion curves in Fig. 2 are evaluated by an eigenfrequency study using the Acoustics module in COMSOL Multiphysics[72]. Floquet–Bloch boundaries are added on the left and right sides of the modeshape geometries in Fig. 2, with perfectly matched layers (PML) top and bottom. The modes above the cut-off are isolated by evaluating the ratio of the integral of the absolute modulus of the pressure field in a region near the scatterer (dashed boxes in Fig. 2) to the same quantity in the rest of the domain. The continuous dispersion curves above the cut-off clearly depend on this threshold parameter, which is tuned until no 'air-box' modes are found; air-box modes can be isolated as their eigenfrequencies shift with the size of the bounding box[73]. Alternatively, inspection of the imaginary part of the eigenvalues (and therefore the quality factor of the associated resonances) can be used to isolate the QNMs[18,20].

Continuous wave measurements
Signal recorded on an oscilloscope (Siglent SDS2352X-E). Acoustic data was recorded with a sampling frequency of 500 kSa s^{-1}, for a total time of 0.28 sec, and with 32 averages.

The experimental procedure was as follows: the microphone was positioned close to the central rod in the 11-cylinder long array. The lattice was driven to a steady state at discrete frequencies (2 to 20 kHz in 50 Hz

steps) and the signal from the microphone recorded. This was repeated at three positions around the central rod and the data averaged. Similar measurements were performed at the same positions without rods for normalisation.

To determine the frequency response of the finite array, the temporal acoustic signals were summed, producing a signal (voltage) as a function of time $V(x_i, t)$ at discrete positions x_i near the central. The data were processed using temporal Fourier transform.

Pulsed measurements

The 80-rod long samples are excited by a tweeter (Kemo L010 Piezo Loudspeaker) mounted within the supporting frame at the mid-height of the rods. The loudspeaker is driven by an arbitrary waveform generator (Keysight 33500B), producing single-cycle Sine–Gaussian pulses centred at $f_c = 16$ kHz, and a broadband amplifier (Thurly Thandar Instruments WA301). The acoustic pressure field is measured with a small aperture microphone (Brüel & Kjær Probe Type 4182 near-field microphone, with a preconditioning amplifier) positioned 2 mm normal to the array direction. Acoustic data are recorded by an oscilloscope (Picoscope 5000a) at sampling frequency $f_s = 312.5$ kHz. The microphone is mounted on a motorised xyz scanning stage (in-house with Aerotech controllers), to map the acoustic signal spatially. An average was taken over 20 measurements at each spatial position to improve the signal-to-noise ratio. The microphone is scanned along the full sample length with 15 points per unit cell step-size in the propagation direction. Acoustic data are analysed using Fourier techniques to obtain the wavenumber–frequency dependence of the propagating waves. The fast-Fourier Transform (FFT, operator $\mathcal{F}$) of the measured signal voltage $V(x, t)$ returns the complex Fourier amplitude in terms of the wavenumber parallel to the surface β and frequency f, $\mathcal{F}_x(|\mathcal{F}_t(V(x, t))|)$. Raw data are presented in Fig. 4 with no windowing or zero-padding in either space or time.

Data availability

The data that supports the findings of this study are available from the corresponding author upon reasonable request.

Code availability

The code that supports the findings of this study are available from the corresponding author upon reasonable request.

References

1. Wilcox, C. H. Scattering theory for diffraction gratings. *Math. Methods Appl. Sci.* **6**, 158 (1984).
2. Porter, R. & Evans, D. V. Rayleigh-Bloch surface waves along periodic gratings and their connection with trapped modes in waveguides. *J. Fluid Mech.* **386**, 233–258 (1999).
3. Peter, M. A. & Meylan, M. H. Water-wave scattering by a semi-infinite periodic array of arbitrary bodies. *J. Fluid Mech.* **575**, 473–494 (2007).
4. Antonakakis, T., Craster, R. V., Guenneau, S. & Skelton, E. A. An asymptotic theory for waves guided by diffraction gratings or along microstructured surfaces. *Proc. R. Soc. A: Math., Phys. Eng. Sci.* **470**, 20130467 (2014).
5. Colquitt, D. J., Craster, R. V., Antonakakis, T. & Guenneau, S. Rayleigh–Bloch waves along elastic diffraction gratings. *Proc. R. Soc. A: Math. Phys. Eng. Sci.* **471**, 20140465 (2015).
6. Bonnet-Bendhia, A.-S. & Starling, F. Guided waves by electromagnetic gratings and non-uniqueness examples for the diffraction problem. *Math. Methods Appl. Sci.* **17**, 305 (1994).
7. Linton, C. M. & McIver, M. The existence of Rayleigh-Bloch surface waves. *J. Fluid Mech.* **470**, 85–90 (2002).
8. Chaplain, G. J., Makwana, M. P. & Craster, R. V. Rayleigh-Bloch, topological edge and interface waves for structured elastic plates. *Wave Motion* **86**, 162 (2019).
9. Brillouin, L. *Wave Propagation in Periodic Structures: Electric Filters and Crystal Lattices*, 2nd ed. (Dover Publications, Inc., New York, 1953).
10. Linton, C. M., Porter, R. & Thompson, I. Scattering by a semi-infinite periodic array and the excitation of surface waves. *SIAM J. Appl. Math.* **67**, 1233 (2007).
11. Thompson, I., Linton, C. M. & Porter, R. A new approximation method for scattering by long finite arrays. *Q. J. Mech. Appl. Math.* **61**, 333 (2008).
12. Porter, R. & Evans, D. Embedded Rayleigh-Bloch surface waves along periodic rectangular arrays. *Wave Motion* **43**, 29 (2005).
13. Bennetts, L. G. & Peter, M. A. Rayleigh-Bloch waves above the cutoff. *J. Fluid Mech.* **940**, A35 (2022).
14. Laude, V. & Wang, Y.-F. Quasinormal mode representation of radiating resonators in open phononic systems. *Phys. Rev. B* **107**, 144301 (2023).
15. Yan, W., Faggiani, R. & Lalanne, P. Rigorous modal analysis of plasmonic nanoresonators. *Phys. Rev. B* **97**, 205422 (2018).
16. Colom, R., McPhedran, R., Stout, B. & Bonod, N. Modal expansion of the scattered field: Causality, nondivergence, and nonresonant contribution. *Phys. Rev. B* **98**, 085418 (2018).
17. Stout, B., Colom, R., Bonod, N. & McPhedran, R. C. Spectral expansions of open and dispersive optical systems: Gaussian regularization and convergence. *N. J. Phys.* **23**, 083004 (2021).
18. Vial, B., Zolla, F., Nicolet, A. & Commandré, M. Quasimodal expansion of electromagnetic fields in open two-dimensional structures. *Phys. Rev. A* **89**, 023829 (2014).
19. Lalanne, P., Coudert, S., Duchateau, G., Dilhaire, S. & Vynck, K. Structural slow waves: parallels between photonic crystals and plasmonic waveguides. *ACS Photonics* **6**, 4 (2018).
20. Lalanne, P. et al. Quasinormal mode solvers for resonators with dispersive materials. *JOSA A* **36**, 686 (2019).
21. Vial, B., Sabaté, M. M., Wiltshaw, R., Guenneau, S. & Craster, R. V. Platonic quasi-normal modes expansion. arXiv preprint arXiv:2407.12042 (2024).
22. Kang, M., Liu, T., Chan, C. & Xiao, M. Applications of bound states in the continuum in photonics. *Nat. Rev. Phys.* **5**, 659 (2023).
23. Hsu, C. W. et al. Observation of trapped light within the radiation continuum. *Nature* **499**, 188 (2013).
24. Hsu, C. W., Zhen, B., Stone, A. D., Joannopoulos, J. D. & Soljačić, M. Bound states in the continuum. *Nat. Rev. Mater.* **1**, 1 (2016).
25. Matsushima, K., Bennetts, L. G. & Peter, M. A. Tracking Rayleigh–Bloch waves swapping between Riemann sheets. *Proc. R. Soc. A* **480**, 20240211 (2025).
26. Bennetts, L. G., Peter, M. A. & Montiel, F. Localisation of Rayleigh–Bloch waves and damping of resonant loads on arrays of vertical cylinders. *J. Fluid Mech.* **813**, 508 (2017).
27. Sheng, P. & van Tiggelen, B. Introduction to wave scattering, localization and mesoscopic phenomena. second edition. *Waves Random Complex Media* **17**, 235 (2007).
28. Maradudin, A. A., Sambles, J. R. & Barnes, W. L. *Modern plasmonics* (Elsevier, 2014).
29. Kravets, V. G., Kabashin, A. V., Barnes, W. L. & Grigorenko, A. N. Plasmonic surface lattice resonances: a review of properties and applications. *Chem. Rev.* **118**, 5912 (2018).
30. Alù, A. & Engheta, N. Theory of linear chains of metamaterial/plasmonic particles as subdiffraction optical nanotransmission lines. *Phys. Rev. B* **74**, 205436 (2006).
31. Markel, V. A. Coupled-dipole approach to scattering of light from a one-dimensional periodic dipole structure. *J. Mod. Opt.* **40**, 2281 (1993).

32. Cherqui, C., Bourgeois, M. R., Wang, D. & Schatz, G. C. Plasmonic surface lattice resonances: theory and computation. *Acc. Chem. Res.* **52**, 2548 (2019).

33. Liu, X.-X. & Alù, A. Subwavelength leaky-wave optical nanoantennas: directive radiation from linear arrays of plasmonic nanoantennas. *Phys. Rev. B* **82**, 144305 (2010).

34. Bulgakov, E. N. & Maksimov, D. N. Light guiding above the light line in arrays of dielectric nanospheres. *Opt. Lett.* **41**, 3888 (2016).

35. Bohren, C. F. & Huffman, D. R. *Absorption and scattering of light by small particles* (John Wiley & Sons, 2008).

36. Yang, Z., Zhang, K., Fang, C. & Hu, J. Non-hermitian bulk-boundary correspondence and auxiliary generalized brillouin zone theory. *Phys. Rev. Lett.* **125**, 226402 (2020).

37. Imura, K.-I. & Takane, Y. Generalized bloch band theory for non-hermitian bulk–boundary correspondence. *Prog. Theor. Exp. Phys.* **2020**, 12A103 (2020).

38. Cummer, S. A., Christensen, J. & Alù, A. Controlling sound with acoustic metamaterials. *Nat. Rev. Mater.* **1**, 1 (2016).

39. Xiong, L. et al. Tracking intrinsic non-hermitian skin effects in lossy lattices. *Phys. Rev. B* **110**, L140305 (2024).

40. Chen, P. Y., Bergman, D. J. & Sivan, Y. Generalizing normal mode expansion of electromagnetic green's tensor to open systems. *Phys. Rev. Appl.* **11**, 044018 (2018).

41. Capers, J. R., Patient, D. A. & Horsley, S. A. R. Inverse design in the complex plane: manipulating quasinormal modes. *Phys. Rev. A* **106**, 053523 (2022).

42. Moore, D. B., Sambles, J. R., Hibbins, A. P., Starkey, T. A. & Chaplain, G. J. Acoustic surface modes on metasurfaces with embedded next-nearest-neighbor coupling. *Phys. Rev. B* **107**, 144110 (2023).

43. Linton, C. M. & Evans, D. V. Integral equations for a class of problems concerning obstacles in waveguides. *J. Fluid Mech.* **245**, 349–365 (1992).

44. Maniar, H. D. & Newman, J. N. Wave diffraction by a long array of cylinders. *J. Fluid Mech.* **339**, 309–330 (1997).

45. Utsunomiya, T. & Taylor, R. E. Trapped modes around a row of circular cylinders in a channel. *J. Fluid Mech.* **386**, 259–279 (1999).

46. Antonakakis, T., Craster, R. V. & Guenneau, S. High-frequency homogenization of zero-frequency stop band photonic and phononic crystals. *N. J. Phys.* **15**, 103014 (2013).

47. Raghavan, L. & Phani, A. S. Local resonance bandgaps in periodic media: theory and experiment. *J. Acoustical Soc. Am.* **134**, 1950 (2013).

48. Zeng, X., Yu, F., Shi, M. & Wang, Q. Fluctuation of magnitude of wave loads for a long array of bottom-mounted cylinders. *J. Fluid Mech.* **868**, 244 (2019).

49. Barnes, W. L. Particle plasmons: why shape matters. *Am. J. Phys.* **84**, 593 (2016).

50. Sieck, C. F., Alù, A. & Haberman, M. R. Origins of Willis coupling and acoustic bianisotropy in acoustic metamaterials through source-driven homogenization. *Phys. Rev. B* **96**, 104303 (2017).

51. Jordaan, J. et al. Measuring monopole and dipole polarizability of acoustic meta-atoms. *Appl. Phys. Lett.* **113** (2018).

52. Melnikov, A. et al. Acoustic meta-atom with experimentally verified maximum Willis coupling. *Nat. Commun.* **10**, 3148 (2019).

53. Hicks, E. M. et al. Controlling plasmon line shapes through diffractive coupling in linear arrays of cylindrical nanoparticles fabricated by electron beam lithography. *Nano Lett.* **5**, 1065 (2005).

54. Rodriguez, S., Schaafsma, M., Berrier, A. & Rivas, J. G. Collective resonances in plasmonic crystals: size matters. *Phys. B: Condens. Matter* **407**, 4081 (2012).

55. Ganesh, M. & Hawkins, S. C. Algorithm 975: TMATROM-a T-Matrix reduced order model software. *ACM Trans. Math. Softw*. **44**, https://doi.org/10.1145/3054945 (2017).

56. Hawkins, S. C. et al. Metamaterial applications of TMATSOLVER, an easy-to-use software for simulating multiple wave scattering in two dimensions. *Proc. R. Soc. A: Math. Phys. Eng. Sci.* **480**, https://doi.org/10.1098/rspa.2023.0934 (2024).

57. Colton, D. & Kress, R. Inverse acoustic and electromagnetic scattering theory. *Appl. Math. Sci.* **93**, 1 (1992).

58. Ganesh, M. & Hawkins, S. C. A numerically stable T-matrix method for acoustic scattering by nonspherical particles with large aspect ratios and size parameters. *J. Acoustical Soc. Am.* **151**, 1978 (2022).

59. Vanel, A. L., Schnitzer, O. & Craster, R. V. Asymptotic network models of subwavelength metamaterials formed by closely packed photonic and phononic crystals. *Europhys. Lett.* **119**, 64002 (2017).

60. Vanel, A. L., Craster, R. V. & Schnitzer, O. Asymptotic modeling of phononic box crystals. *SIAM J. Appl. Math.* **79**, 506 (2019).

61. Skigin, D. C., Veremey, V. V. & Mittra, R. Superdirective radiation from finite gratings of rectangular grooves. *IEEE Trans. Antennas Propag.* **47**, 376 (1999).

62. Skigin, D. C. Transmission through subwavelength slit structures with a double period: a simple model for the prediction of resonances. *J. Opt. A: Pure Appl. Opt.* **11**, 105102 (2009).

63. Sugino, C., Xia, Y., Leadenham, S., Ruzzene, M. & Erturk, A. A general theory for bandgap estimation in locally resonant metastructures. *J. Sound Vib.* **406**, 104 (2017).

64. Langfeldt, F. On the validity of periodic boundary conditions for modelling finite plate-type acoustic metamaterials. *J. Acoustical Soc. Am.* **155**, 837 (2024).

65. Barlow, H. E. M. & Karbowiak, A. An experimental investigation of the properties of corrugated cylindrical surface waveguides. *Proc. IEE-part III: Radio Commun. Eng.* **101**, 182 (1954).

66. Hurd, R. A. The propagation of an electromagnetic wave along an infinite corrugated surface. *Can. J. Phys.* **32**, 727 (1954).

67. Pendry, J. B., Martin-Moreno, L. & Garcia-Vidal, F. J. Mimicking surface plasmons with structured surfaces. *Science* **305**, 847 (2004).

68. Hibbins, A. P., Evans, B. R. & Sambles, J. R. Experimental verification of designer surface plasmons. *Science* **308**, 670 (2005).

69. Evans, D. V. & Porter, R. Penetration of flexural waves through a periodically constrained thin elastic plate in vacuo and floating on water. *J. Eng. Math.* **58**, 317 (2007).

70. Brekhovskikh, L. M. Surface waves in acoustics. *Sov. Phys. Acoust.* **5**, 3 (1959).

71. Kelders, L., Allard, J. F. & Lauriks, W. Ultrasonic surface waves above rectangular-groove gratings. *J. Acoust. Soc. Am.* **103**, 2730 (1998).

72. COMSOL Multiphysics® v. 6.2 www.comsol.com/ (COMSOL AB, Stockholm, Sweden).

73. Chaplain, G. J. *Metasurfaces for wave control: redirection, rainbow and focussing phenomena in elasticity, electromagnetism and acoustics*, Ph.D. thesis, Imperial College London (2021).

Acknowledgements

Author contributions

M.A.P. and L.G.B. developed the theory of generalised RB waves. G.J.C. and T.A.S. performed FE simulations and carried out the experiments, and dealt with post-processing. S.C.H. performed the MWS simulations and analysis. All authors contributed to the interpretation of results and writing of the manuscript.

Competing interests

The authors declare no competing interests.

Additional information